

# Field Installation, Splicing, and Flexural Testing of Hybrid FRP/Concrete Piles

by K. Helmi, A. Fam, and A. Mufti

**Synopsis:** Concrete-filled fiber-reinforced polymer (FRP) tubes (CFFT) are becoming increasingly popular in pile applications. An experimental program was undertaken to address the drivability and effect of driving forces on CFFT piles as well as the use of splices. In this program, four full-scale piles, 357 mm in diameter, and 13.7 m long, including a spliced pile, were driven into the ground and then extracted. The piles were cut into 6 m portions that were used for beam tests on spliced and unspliced specimens and 0.3 m portions used for material characterization of the FRP tube and push-off tests to evaluate the bond strength between the concrete core and FRP tube. Test results were compared to those of control specimens, which were not subjected to driving forces. In total, six beam tests, 28 push-off tests and 54 tension coupon tests were conducted. Test results indicate that driving forces have marginal effect, about 5% reduction, on the flexural strength of both unspliced and spliced CFFT piles, on bond strength and on the tensile strength of the FRP tube. It is also shown that the mechanical splice used in this study performed well and was capable of developing a moment resistance, 7% higher than that of the CFFT pile.

**Keywords:** bending; bond; CFFT; concrete-filled; driving; FRP tubes; pile; splices

ACI student member **Karim Helmi** is a Ph.D. Candidate at the University of Manitoba, Winnipeg, MB, Canada. He received his B.Sc. degree from the Faculty of Engineering, Alexandria University, Alexandria, Egypt; and his M.A.SC. from the University of Windsor, Windsor, ON, Canada.

ACI Member **Amir Fam** is an Assistant Professor and Canada Research Chair in Innovative and Retrofitted Structures at Queen's University, Canada. He is a voting member of ACI Committee 440, FRP Reinforcement and Co-Chairman of Sub-Committee 440-J, FRP Stay-in-Place Formwork. His research interests include applications of FRP in new construction and retrofit of existing structures.

ACI Member **Aftab Mufti** is a Professor of Civil Engineering at the University of Manitoba, Canada. He is the President of ISIS Canada Research Network, the President of ISHMII and the Chair of the Technical Subcommittee of the Canadian Highway Bridge Design Code. His research interests include FRPs, FEM, bridge engineering, structural health monitoring and Civionics. Dr. Mufti is the recipient of 16 awards.

### INTRODUCTION

A large part of the civil infrastructure is approaching the end of its design life. Additionally, advances in industry and increased populations have led to an increased demand on existing infrastructure such as bridges. This has led engineers and scientists to search for innovative solutions that would provide alternatives for conventional materials and systems that have a longer life and require less maintenance. One such innovation, which is becoming an attractive alternative for piles and bridge pier applications, is concrete-filled FRP tubes (CFFT), especially in corrosive and marine environments (Fam et al 2003 and Pando et al 2003). CFFTs are easy to construct and are resistant to corrosion and attack by marine organisms. Although CFFTs have been extensively studied in the past decade, studies have mostly been focused on characterizing the short-term monotonic behavior of CFFT piles in bending and under axial loads. The effect of driving forces on strength of CFFT piles and development of reliable splices are two areas that need further research. The drivability of CFFT piles has been studied analytically (Ashford and Jakrapiyanum 2001 and Iskander et al 2001) and in the field by monitoring the driving process (Mirmiran et al 2002 and Pando et al 2003), however, the effect of residual damage on flexural strength of the piles was not assessed as the piles were never extracted from the ground. Development of reliable splices for CFFT piles is particularly important since FRP tubes have limited lengths due to manufacturing and transportation constraints. Additionally, pile driving equipment may provide additional restrictions on the length of piles they can accommodate. Parvathaneni et al (1996) produced a 13.7 m long CFFT pile using three 4.6 m long units, spliced using short steel tubing, 0.6 m long, which matched the inside diameter of the GFRP tubes. Mirmiran et al (2002) constructed a splice by machining the wall thicknesses of the two units to half the thickness, forming a 0.6 m long male-female splice. The overlap regions were wetted with epoxy in the field before fitting. Splicing using these systems had to be done before the driving of the piles and do not allow for splicing during driving.

An experimental program was undertaken at the University of Manitoba to address these areas of research needs. The program included driving of four CFFT piles, including a pile that was spliced during driving. The piles were then extracted from the ground and portions were cut and tested in bending to evaluate the effect of driving forces on flexural strength of CFFT unspliced and spliced piles. Additional ancillary tests, namely tensile coupon tests and push-off tests, were conducted to evaluate the effect of driving forces on the tensile strength of FRP tubes and on the bond strength between the concrete core and FRP tube.

## **EXPERIMENTAL PROGRAM**

Four, 357 mm diameter and 13.7 m long piles, one of which was spliced, were driven into the ground and then extracted. The piles were then cut into 6 m and 0.3 m long portions that were used for beam tests, tensile coupon tests, and push-off tests. Test results were compared to those of control specimens, which were not subjected to driving forces. Beam tests conducted on the 6 m long portions were also used to evaluate the structural performance of the splices.

### **Description of GFRP Tubes and Pile Specimens**

Filament-wound E-Glass/Epoxy FRP (GFRP) tubes were used in this study. The dimensions and mechanical properties of the tubes, as provided by the manufacturer, are presented in Table 1. The stacking sequence of the different layers in the tubes is [87.3/1.4/87.3/1.4/87.3/1.4/87.3/1.4/87.3], where the [87.3] represents the angle between hoop layers and the longitudinal axis, and the [1.4] represent the angle between longitudinal layers and longitudinal axis. The inner surface of the tubes has small circumferential ridges of about 0.3 mm projection and spaced at about 9 mm in the longitudinal direction.

The tubes were provided for this study in two lengths, namely 13.7 m and 6 m. Approximately 10.7 m of each of the 13.7 m long tubes has a rough outer surface to enhance skin friction with the soil, while the rest of the lengths of the tubes have a smooth surface. Four, 13.7 m long tubes were used to fabricate the piles that were driven into the ground, which are identified as piles P1 to P4. The tube used for pile P3 was cut into two sections of lengths 10.7 and 3 m to form a spliced pile. The 6 m tubes were used to manufacture the control specimens, which were not driven, and are identified as piles C1 to C5. Piles C4 and C5 were cut into two sections each, to provide spliced control specimens.

### **Concrete**

The concrete mixture used for filling the GFRP tubes included super plasticizers to achieve high workability and insure a complete filling of the tubes. Additionally, an expansive agent was used to compensate for the shrinkage of concrete after hardening and prevent separation of the concrete core from the tubes. Standard cylinders were prepared and tested according to ASTM C39 [ASTM C39-96]. The average strength of the concrete cylinders was 59 MPa.

**Splices**

The splice used in this program consists of two 50 mm thick circular plates, as shown in Figure 1(a). Eight, 19 mm diameter and 2.7 m long, reinforcing steel bars with threaded ends are screwed into eight threaded holes in the plates. Each plate is installed at the end of one GFRP tube such that the bars are embedded inside the tubes, and bonded to the concrete core after filling the tubes. Each plate has four T-shaped grooves around its perimeter, as shown in Figure 1(b). To form a splice, the two parts of the pile are placed together such that the T-grooves are aligned to form an I-shaped groove. An I-shaped key is then inserted in each of the grooves to connect both ends of the splice. Part of the side of each edge of the T-grooves is originally machined to form a lip. After inserting the keys, these lips are hammered towards the keys to secure the keys in place and prevent their movement during the driving process.

**Fabrication of CFFT Piles**

The specimens were fabricated at LaFarge Canada precast plant in Winnipeg, Manitoba, Canada. The tubes were plugged at both ends using circular wooden plugs. A 100 mm diameter circular hole was provided in one plug in order to facilitate pumping of concrete into the tube. The steel splice plates in pile specimens P3, C4, and C5 were used as bottom plugs. The tubes were then put on an inclined surface and concrete was pumped through the upper end plug, as shown in Figure 2. After the tubes have been filled, the opening at the top plug was then sealed.

**Driving and Extraction of CFFT Piles**

After curing for 21 days, piles P1 to P4 were shipped to the yard of Agra Foundations Company in Winnipeg, Manitoba, Canada, and were driven into the ground (firm silty clay), using the same procedure and equipment conventionally used for driving pre-cast prestressed concrete piles. A Linkbelt LB520 hammer with a rated energy of 3665 kg.m was used for pile driving. The driving force was applied to the entire cross-section, including the tube and concrete core, using a 50 mm thick wooden cushion. Piles P1, P2 and P3 were driven to the end of their lengths. Afterwards, a short steel mandrel was added and the driving continued to the refusal depth of the soil, which was about 14.3 m. Pile P4 was driven to a depth of 12 m only, in order to perform a skin friction test. Figure 3(a) show the pile driving process. For spliced pile P3, the longer section was first driven all the way into the ground, the shorter section was then connected through the splice and driving was continued, as shown in Figure 3(b).

In order to extract the driven piles from the ground, four holes were drilled around each pile, using a 600 mm diameter auger to relieve the soil pressure, as shown in Figure 4. The piles were then pulled out of the ground using a crane.

**Description of Test Specimens**

CFFT beam specimens – The objectives of this group of tests are: (1) to examine the effect of driving stresses on the flexural behavior of CFFT piles, (2) to evaluate the structural performance and adequacy of the splice described earlier, and (3) to examine the effect of driving stresses on this type of splices. It is worth noting that CFFT piles are

mostly used in corrosive marine environments and are generally subjected to high bending and minimum axial compression loads, as in the case of fender piles.

Six beam specimens were cut from the piles using a diamond tip concrete saw, as shown in Figure 5, including three spliced and three unspliced specimens. Table 2 presents a summary of the beam specimens. The specimens are given identification codes such that 'B' and 'S' indicate unspliced and spliced specimens, 'P' and 'C' indicate driven and control specimens, 'U' and 'L' indicate specimens cut from the upper and lower ends of the driven piles and 'x' and '+' represent the orientations of the four keys in spliced specimens. Table 2 also shows the piles, from which, specimens are cut.

**CFFT push-off specimens** – The objective of these tests is to evaluate the bond strength between the concrete core and GFRP tube and examine any negative effects of driving forces on bond strength, at three locations along the length of driven piles, namely at top, middle and bottom. The specimens used for these tests are 300 mm long and were cut from both the control and driven piles. Table 3 provides summary of the different specimens, where 'C' and 'P' indicate control and driven piles and 'T', 'M' and 'B' indicate top, middle, and bottom of the pile. For example, C1B indicates a specimen cut from control pile C1 from the bottom end and P4M1 and P4M2 indicate two similar specimens cut from the middle of driven pile P4.

**GFRP tension coupon specimens** – The objective of these tests is to determine the effect of driving forces on the GFRP tube by measuring any variation that occurs in the tensile strength of the GFRP tube. Three longitudinal strips, 25 x 200 mm were cut from the push-off specimens taken from top and bottom parts of the piles, after the tests were concluded. The specimens were then machined into a dog bone shape according to ASTM D 638, as shown in Figure 6. As indicated in Table 4, specimens were given same identifications as their respective push-off specimens.

### **Test Setups and Instrumentation**

The unspliced beams were tested under four point bending over a span of 5 m and the distance between the loads was 1 m, as shown in Table 2 and Figure 7(a). The spliced beams, on the other hand, were tested under three point bending over a span of 4.5 m and the splice was positioned at a distance of 550 mm from mid span, as shown in Table 2 and Figure 7(b). This setup was chosen so that the splice would be subjected to a combined high bending moment and shear force. All test beams were simply supported on roller supports. A 5000 kN MTS testing machine was used to apply the load in stroke control. Linear variable displacement transducers (LVDTs) were used to measure the deflection at mid-span and at the splice location in spliced beams. LVDTs were also mounted on the ends to measure slip between the concrete core and the GFRP tube, as shown in Figure 8. The load was measured using a load cell integrated within the testing machine. A Data Acquisition System was used to record data continuously during testing.

For push-off tests, specimens were positioned on top of a 300 mm diameter flat steel plate such that it would be in contact with the concrete core only. On top of the specimen, a steel plate with a circular void slightly larger than the inner diameter of the GFRP tube

was positioned such that it would rest on the tube only and would not bear on the concrete during the test. The Load was applied on the plate using a 1000 kN MTS machine. A minimum of three LVDTs were positioned on top of the plate to measure the slip during the test. The Load was measured through a load cell integrated with the testing machine. The data was continuously recorded during the test using a Data Acquisition System. Figure 9 shows the push-off test setup and instrumentation.

For the GFRP tension coupon tests, a 134 kN Baldwin universal testing machine was used. The specimens were gripped using a wedge grip system and the load was applied monotonically up to failure. The maximum load was recorded at failure.

## **TEST RESULTS AND DISCUSSIONS**

### **CFFT Beam Tests**

Figure 10(a) shows the load-deflection behavior for the three unspliced CFFT specimens, BC, BPU and BPL. The cracking load, as indicated by control specimen BC, is very low (18 kN), compared to the ultimate load (200 kN). Also, the stiffness of the specimens exhibits gradual reduction up to failure. This is attributed to the non-linear characteristics of the concrete core as well as the GFRP laminate structure of the tube. The GFRP layers in the circumferential direction fail earlier than the longitudinal layers, resulting in softening of the GFRP tube, which was also reported by Fam et al (2002). The behavior also shows several minor load drops, which could be attributed to gradual cracking of the concrete core or minor slip between concrete and GFRP tube. These load drops are small in magnitude, which suggests that adequate bond between the tube and the concrete was maintained. This was also confirmed by the insignificant slip measurement, as will be discussed. By comparing the behavior of the three specimens it is noticed that the two specimens from the upper and lower ends of the driven pile, specimens BPU and BPL, did not show distinct cracking points as the control specimen BC, which indicate that both specimens were cracked during the driving process. Most importantly is that the driving process appears to result in only a very small reduction (5.5%) in the ultimate moment capacity of the pile. This minor reduction is more pronounced in the upper end of the pile. The ultimate moment based on maximum loads for specimens BC, BPL and BPU were 200, 195 and 189 kN.m, respectively.

Figure 10(b) shows the load-deflection behavior of the spliced CFFT beam specimens SCx, SC+, and SPUx. At load levels of 175 to 200 kN, the specimens exhibit considerable reduction in stiffness, as a result of initiation of yielding in the bottom steel keys and rebar of the splices. The behavior of control specimens SCx and SC+ indicates that the orientation of the splice keys has a very small effect on ultimate load, where the '+' pattern results in a slightly higher load than the 'x' pattern. The behavior of the spliced beam from the upper end of the driven pile, SPUx, indicates that driving forces have very small effect (4%) on the strength of spliced piles. The ultimate moments reached at the splices for specimens SCx, SC+ and SPUx at failure were 215, 221, and 207 kN.m, respectively. All these values have slightly exceeded the ultimate moment capacity of the unspliced specimens BC, BPU and BPL, by about 7%. As such, this type of splice was successful, and in fact optimum, in developing the flexural strength of the

CFFT pile. It should be noted; however, that the length of rebar, used to anchor the end plates, is over designed in this study, to avoid pull-out bond failure. Further research could lead to optimizing the rebar embedment length, especially when realizing the beneficial confinement effect of the tube. As will be discussed later, failure of spliced specimens occurred at splice location and not at the maximum moment at mid-span. This is attributed to the presence of the 8-19 mm rebar, which increased the moment resistance of the CFFT. For example, specimen SCx reached 291 kN.m at mid-span, which is significantly higher than the moment resistance of unspliced specimen BC (200 kN.m).

The load-end slip diagrams for the unspliced control specimen BC is shown in Figure 11(a). A jump appears at about 95 kN load in the slip measured at one end and corresponds to a load drop in the load-deflection curve. Near failure, the slip increased at higher rate at the other end, suggesting some minor loss of bond. However, the total measured slip in any of the unspliced beams did not exceed 0.025 mm, which indicates excellent composite action. The spliced beam specimens also experienced some slip near failure, as evident in Figure 11(b) for specimen SCx. The total slip prior to failure did not exceed 0.11 mm, which is also a very small value, yet higher than that measured in unspliced beams, due to the shorter span and higher loads achieved in this case.

The unspliced specimens failed in tension within the constant moment region. Several snapping sounds were heard as the fibers began to rupture, immediately followed by a sudden failure, as shown in Figure 12(a). The specimens failed by rupture of the longitudinal fibers in tension, accompanied by splitting of the circumferential fibers. The spliced specimens, on the other hand, failed also suddenly but due to fracture of the reinforcement bars of the splice at the threaded ends mounted into the steel plates. Failure was accompanied by some slippage between the concrete core and the GFRP tube at the interface with the steel plate and formation of a small crushed zone on the top part of the tube, as shown in Figure 12(b).

### **CFFT Push-Off Tests**

The maximum measured load and maximum bond stress for each specimen are presented in Table 3. The bond stress  $\sigma$  is calculated using the following formula:

$$\sigma = \frac{P}{\pi d_i (h - s)} \quad (1)$$

Where  $P$  is the load,  $d_i$  is the inner diameter of the tube,  $h$  is the height of the specimen, and  $s$  is the slip. In general, the bond strength ranged from 0.51 to 0.82 MPa. By grouping the specimens into control specimens and specimens cut from top, middle and bottom sections of the piles, and taking average while including only results within average  $\pm 15\%$ , some observations could be made. Specimens cut from the top and bottom ends of the driven piles suffer some loss in bond strength, compared to central specimens; however this loss is less than 5%. Specimens from middle sections indicate that bond strength seems not to be affected by driving forces.

The load-slip curves for three of the push-off specimens are plotted in Figure 13. All specimens experience an initial linear relation, followed by a sudden load drop, in some

of the specimens. The load reaches a peak value and then shows a series of peaks and valleys, which are quite distinct and easily recognized in some specimens, more than others. The distance from peak to peak or valley to valley for all specimens, however, is almost constant and has a value of about 9 mm. This value is equal to the spacing of the internal ribs in the inner surface of the tubes. This behavior indicates that once friction and adhesion between the concrete core and tube are broken, usually at very small values of slip, the mechanical interlock mechanism becomes quite effective and as slip progresses, the series of peaks and valleys correspond to the concrete core riding over the ridges in a progressive manner. It is important to note that the bond strength, reflected by the peak loads, is maintained, even at very large values of slip (25 mm). It is concluded that internal ribs enhance the bond substantially and prevents total loss of bond strength once the maximum friction and adhesion strengths have been reached.

### **GFRP-Tension Coupon Tests**

The ultimate loads recorded for all tension specimens are presented in Table 4. By grouping the specimens cut from control specimens and coupons cut from top and bottom ends of the driven piles and taking the average, for results within average  $\pm 15\%$ , it could be observed that the reduction in strength due to pile driving does not exceed 5%, compared to control specimens. It should be noted, however, that the measured tensile strength using the coupon tests is about 237 MPa, which is lower than the value reported by the manufacturer and given in Table 1. This is attributed to the failure mode of the coupons, which occurred prematurely due to fiber pull-out at a 0.014 strain, as shown in Figure 6, rather than rupture in tension at 0.022 strain as occurred in the beams. The fiber orientation at an angle with respect to the longitudinal axis of the coupons resulted in discontinuity of some of the fibers between the gripping ends.

## **SUMMARY AND CONCLUSIONS**

Four full-scale CFFT piles, including a spliced pile, were driven using conventional pile driving equipment and procedure and were then extracted from the ground. Driving forces were applied to the entire cross-section, including concrete core and tube. Three Beam specimens, of which one included a splice, were cut from the piles and tested in flexure. Test results were compared with those obtained from additional three CFFT beam tests conducted on control (undriven) specimens. A total of 28 push-off tests and 54 tension coupon tests were also conducted on specimens cut from the control and driven piles, from various locations along the pile length. The following conclusions are drawn:

1. Driving of CFFT piles, using conventional methods, is quite feasible. The driving stresses have marginal effect, about 5% reduction, on the flexural strengths of both the CFFT pile and the splice and appears to have no effect on the flexural stiffness of CFFT piles.
2. The mechanical splice used in this study was successful and provided 7% higher moment capacity than that of the CFFT pile it self. Further research may be needed, however, to optimize the length of anchor rebar of the splice, given the advantage of confinement provided by the FRP tube.



3. The orientation of the keys used in the splice has insignificant effect on moment capacity. The '+' pattern showed only 2% higher moment than the 'x' pattern.
4. Driving stresses have marginal effect (about 5% reduction) on bond strength between the concrete core and FRP tube. This effect is pronounced only in the upper and lower ends of the piles. Internal ribs in the tube's inner surface maintain adequate mechanical bond strength, after friction and adhesion strengths are overcome.
5. Tensile strengths of GFRP tubes, obtained using ASTM 638 standard dog-bone coupons, could be highly underestimated, particularly for tubes filament-wound using large winding angles. Failure in this case is due to fiber pull-out rather than fiber rupture. For a relative comparison, this testing method has shown that driving stresses has marginal effect on the tensile strength of GFRP tubes, about 5% reduction.

## REFERENCES

ASTM C39-96 "Standard Test Method for Compressive Strength of Cylindrical Concrete Specimens."

ASTM D 638-91 "Standard Test Method for Tensile Properties of Plastics."

Ashford, S. A. and Jakrapiyanum, W. (2001) "Drivability of FRP Composite Piling," *Journal of Composites for Construction*, 5(2):58-60.

Fam, A., Flisak, B. and Rizkalla, S. (2002) "Experimental and Analytical Modeling of Concrete Filled Fiber Reinforced Polymer Tubes Subjected to Combined Bending and Axial Loads," *ACI Structural Journal*, 100(4):499-509.

Fam, A., Greene, R. and Rizkalla, S. (2003) "Field Applications of Concrete-Filled FRP Tubes for Marine Piles", *Field Application of FRP Reinforcement: Case Studies, ACI Special Publication*, SP-215-9:161-180.

Pando, M., Fam, A., Lesko, J. and Filz, G. (2003) "New Bridge Piers Using Load Bearing Concrete-Filled GFRP Tubes", *Field Application of FRP Reinforcement: Case Studies, ACI Special Publication*, SP-215-10:181-200.

Iskander, M., Hanna, S. and Stachula, A. (2001), "Drivability of FRP Composite Piling," *Journal of Geotechnical and Geoenvironmental Engineering*, 127(2):169-176.

Mirmiran, A., Shao, Y., and Shahawy, M. (2002) "Analysis and Field tests on the Performance of Composite Tubes under Pile Driving Impact," *Composite Structures*, 55(2):127-135.

Parvathaneni, H. K., Iyer, S. L., and Greenwood, M. (1996) "Design and Construction of Test Mooring Pile using Superprestressing," *Proceedings of Advanced Composite Materials in Bridges and Structures, Montreal*, pp. 313-324.

Table 1 — Dimensions and mechanical properties of tubes

Outer Diameter (mm)	367
Total wall thickness (mm)	5.7
Structural wall thickness (mm)	4.8
Longitudinal modulus (GPa)	23.1
Longitudinal tensile strength (MPa)	402

Table 2 — CFFT beam specimens

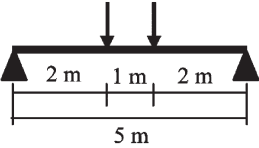

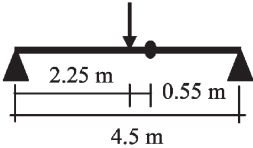


Specimen ID	Source pile	Condition	Splice position	Test setup
BC	C2	Control	No splice	
BPU	P2	Driven		
BPL	P2	Driven		
SCx	C4	Control		
SC+	C5	Control		
SPUx	P3	Driven		

Table 3— Results of CFFT push-off tests

Group	Specimen ID	Max load (kN)	Max stress (MPa)	Average load (kN)	Average stress (MPa)
Specimens from <b>control</b> (undriven) specimens	C1B	244.9	0.769	199.7	0.631
	C1T	202.9	0.655		
	C2B	193.2	0.625		
	C2T	222.3	0.702		
	C3B	162.7	0.514		
	C3T1	174.6	0.544		
	C3T2	197.5	0.608		
Specimens from <b>top</b> of driven piles	P1T1	214.8	0.672	184.7	0.571
	P1T2	245.9	0.760		
	P2T1	186.2	0.556		
	P2T2	164.5	0.519		
	P4T1	166.6	0.522		
	P4T2	221.2	0.685		
	P4T3	245.4	0.743		
Specimens from <b>middle</b> of driven piles	P4T4	229.1	0.710		
	P1M	174.1	0.530	197.0	0.600
	P2M	185.7	0.562		
	P3M	168.4	0.518		
	P4M1	261.3	0.826		
Specimens from <b>bottom</b> of driven piles	P4M2	231.1	0.706		
	P1B1	149.5	0.535	183.2	0.562
	P2B2	264.4	0.825		
	P3B1	176.2	0.548		
	P3B2	171.8	0.527		
	P4B1	176.8	0.549		
	P4B2	208.0	0.622		
	P4B3	238.9	0.731		
	P4B4	238.1	0.727		

Table 4—Results of GFRP tension coupon tests

Control (undriven)		Top (driven)		Bottom (driven)	
Specimen ID	Stress (MPa)	Specimen ID	Stress (MPa)	Specimen ID	Stress (MPa)
C1B	235.1	P1T1	233.0	P1B2	210.1
	239.5		222.1		250.4
	228.6		230.8		244.6
C2B	235.1	P1T2	239.5	P1B1	207.9
	241.3		206.1		192.3
	254.0		214.1		272.9
C3B	249.3	P4T1	242.0	P2B2	230.1
	219.5		234.4		227.2
	250.4		190.9		248.6
C1T	220.0	P4T2	217.4	P2B1	223.9
	238.8		248.2		201.0
	252.4		235.1		271.8
C3T1	198.8	P2T1	238.1	P4B2	219.5
	262.3		244.6		246.4
	233.0		225.0		196.7
C3T2	242.3	P2T2	241.0	P4B1	227.5
	236.0		236.2		234.1
	213.9		244.2		220.6
Average stress (MPa)	236.8	Average stress (MPa)	232.5	Average stress (MPa)	230.1

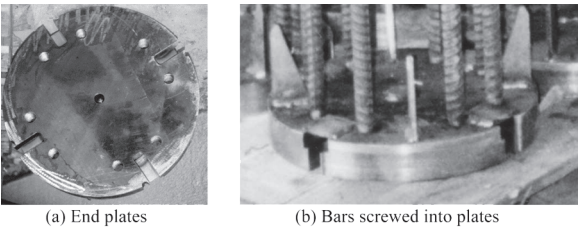


Figure 1—Splice details



Figure 2—Casting concrete into GFRP tubes

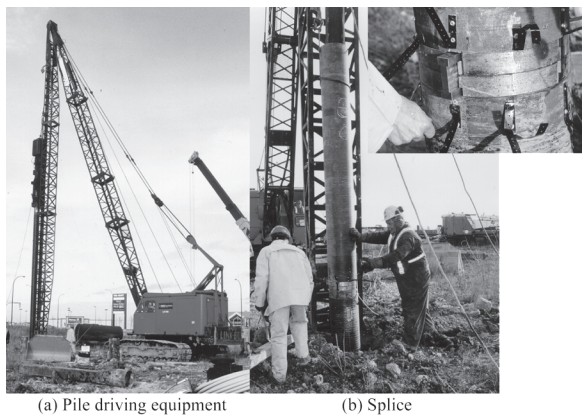


Figure 3—Driving and splicing of CFFT piles



Figure 4—Extraction of CFFT piles



Figure 5—Cutting of test specimens from CFFT Piles

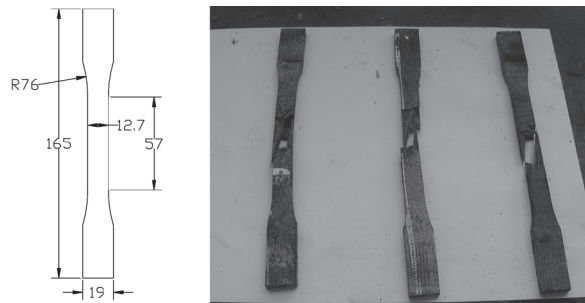
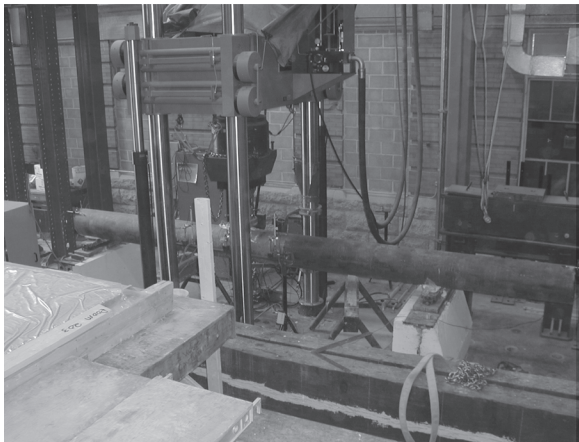


Figure 6—Typical GFRP tension coupons



(a) Unspliced CFFT beam test (four point bending)



(b) Spliced CFFT beam test (three point bending)

Figure 7—Test setups for CFFT beam specimens

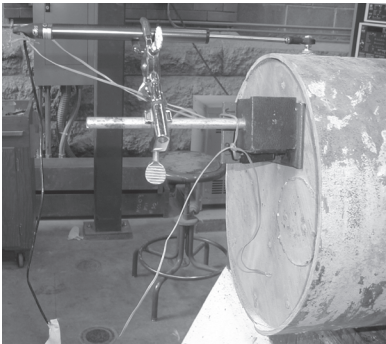


Figure 8—Instrumentation for measuring end slip

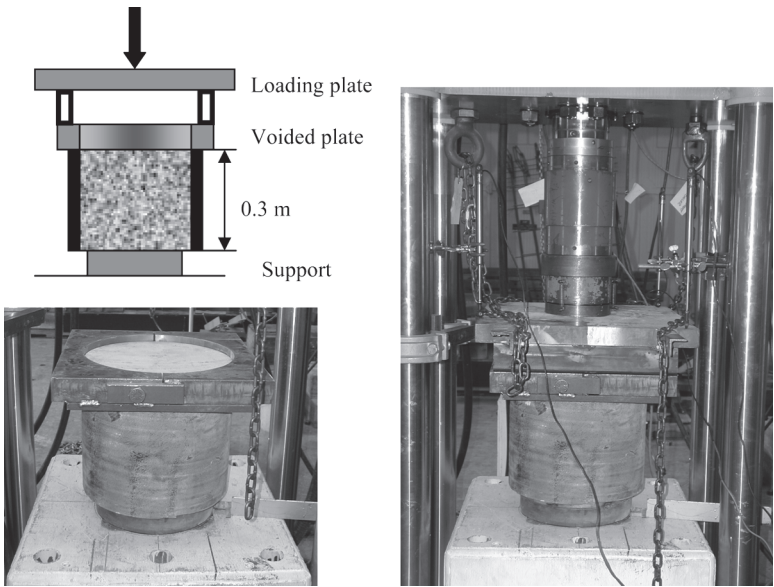
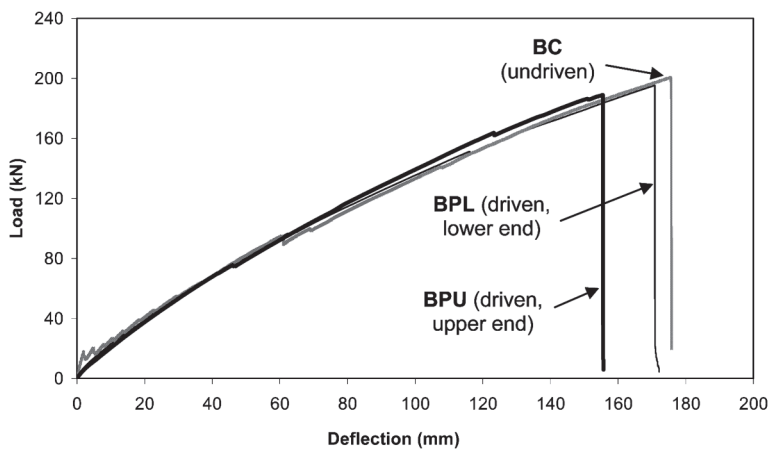
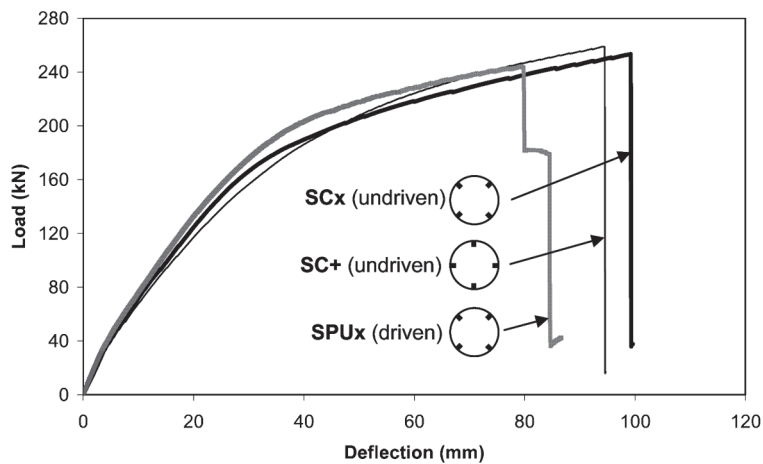


Figure 9—CFFT Push-off test setup



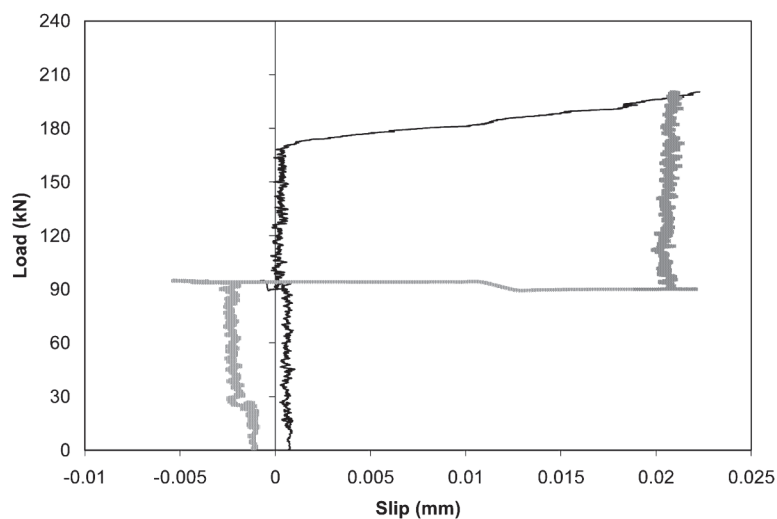
(a) Unspliced CFFT beams



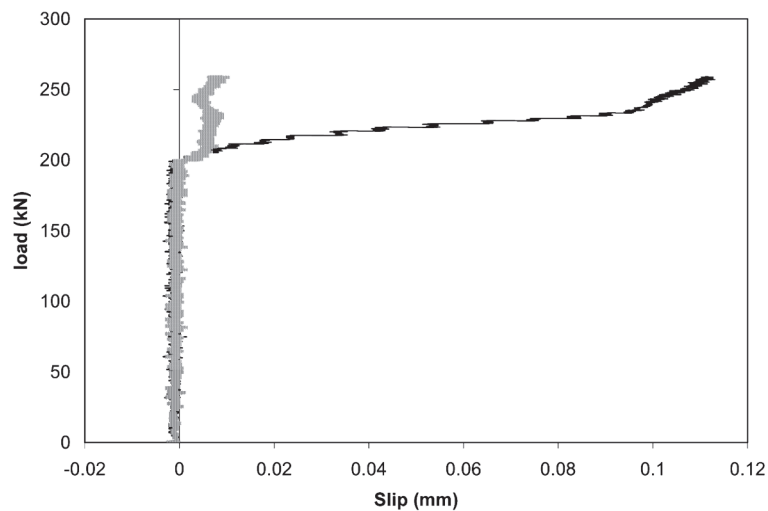
(b) Spliced CFFT beams

Figure 10—Load-deflection behavior of CFFT test beams





(a) Unspliced control specimen BC



(b) Spliced control specimen SCx

Figure 11—Load-slip behavior of CFFT beams

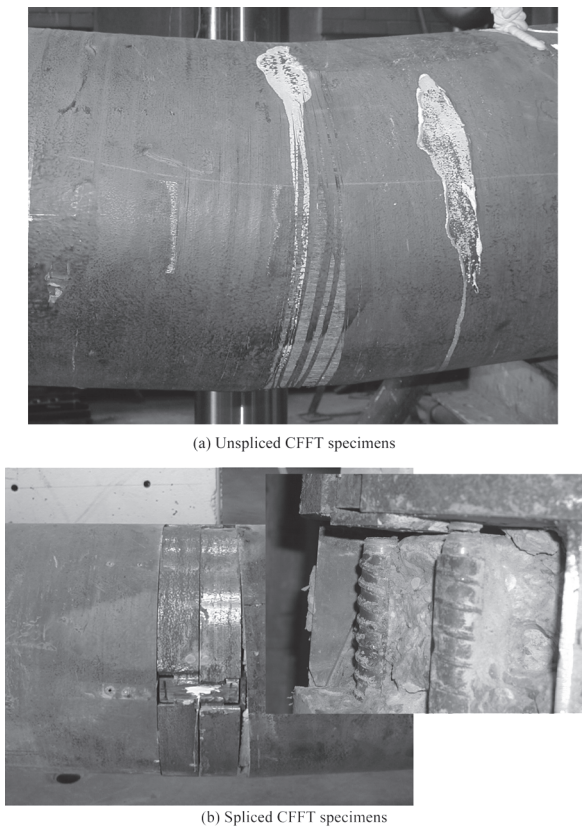


Figure 12—Failure modes of CFFT beams

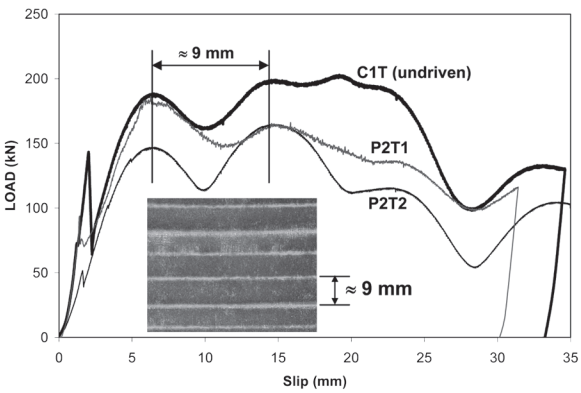


Figure 13—Load-slip behavior of three push-off specimens